The Journal of Experimental Biology 200, 543–556 (1997)
Printed in Great Britain © The Company of Biologists Limited 1997
JEB0423

DRAGONFLY FLIGHT

I. GLIDING FLIGHT AND STEADY-STATE AERODYNAMIC FORCES

J. M. WAKELING* AND C. P. ELLINGTON
Department of Zoology, University of Cambridge, Downing Street, Cambridge CB2 3EJ, UK

Accepted 28 October 1996

Summary

The free gliding flight of the dragonfly *Sympetrum sanguineum* was filmed in a large flight enclosure. Reconstruction of the glide paths showed the flights to involve accelerations. Where the acceleration could be considered constant, the lift and drag forces acting on the dragonfly were calculated. The maximum lift coefficient (C_L) recorded from these glides was 0.93; however, this is not necessarily the maximum possible from the wings. Lift and drag forces were additionally measured from isolated wings and bodies of *S. sanguineum* and the damselfly *Calopteryx splendens* in a steady air flow at Reynolds numbers of 700–2400 for the wings and 2500–15 000 for the bodies. The maximum lift coefficients ($C_{L,max}$) were 1.07 for *S. sanguineum* and 1.15 for *C. splendens*, which are greater than those recorded for all other insects except the locust. The drag coefficient at zero angle of attack ranged between 0.07 and 0.14, being little more than the Blassius value predicted for flat plates. Dragonfly wings thus show exceptional steady-state aerodynamic properties in comparison with the wings of other insects. A resolved-flow model was tested on the body drag data. The parasite drag is significantly affected by viscous forces normal to the longitudinal body axis. The linear dependence of drag on velocity must thus be included in models to predict the parasite drag on dragonflies at non-zero body angles.

Key words: dragonfly, damselfly, *Sympetrum sanguineum*, *Calopteryx splendens*, gliding, lift, drag.

Introduction

During gliding, the air flow over an animal can be considered to be steady, and the forces acting on the wings can be readily measured and predicted. Gliding is an uncommon mode of insect flight; however, studies of the steady-state aerodynamic performance of the wings are still useful for analyses of flapping flight. Flapping flight has typically been considered using quasi-steady analyses (e.g. Osborne, 1951; Weis-Fogh, 1973; Ellington, 1984*b*; Dudley and Ellington, 1990) in which the forces acting on a wing are calculated as if the wing were in a steady flow at each instant. Where the quasi-steady assumptions prove inadequate, new methods of lift generation are implicated.

Dragonflies commonly glide as part of their natural flight repertoire. Insects that glide frequently, dragonflies, locusts and butterflies, spend long periods on the wing and so may benefit from the lower costs of gliding compared with flapping flight. However, the inability to alter their wing span or area leaves insects little control over their gliding performance, and this may explain why they do not widely employ gliding as a mode of flight (Spedding, 1992). One reason for the frequent gliding flights of dragonflies may be thermoregulatory (Heinrich, 1993). Gliding enables dragonflies to benefit from convective cooling by moving quickly through the air without extra heat production by the thoracic flight muscles (May, 1976, 1978). May (1976, 1978) observed that the frequency of gliding flights increased for *Tramea carolina* with increasing ambient temperature, and Hankin (1921), Corbet (1983), Polcyn (1988) and May (1995) also noted the increased incidence of gliding flights for *Anax* and *Hemianax* species on hot, sunny days.

During steady gliding flight, the resultant of the lift and drag acting on the dragonfly balances its weight, and these aerodynamic forces can be calculated from measurements of its glide angle, glide speed and body mass. If the gliding is not steady, lift and drag can still be determined if the accelerations and thus the unbalanced force are accounted for. In the present study, *Sympetrum sanguineum* performed repeated free gliding flights in a warm flight enclosure. These flights were filmed using a pair of synchronised video cameras aligned along orthogonal axes, and the glide path was reconstructed, allowing the lift and drag forces to be calculated. These forces represent the total lift and drag acting on the dragonfly body and wings, but the forces are not evenly spread over these parts; typically, the wings generate virtually all of the total lift and the majority

*Present address: Gatty Marine Laboratory, School of Biological and Medical Sciences, University of St Andrews, St Andrews, Fife KY16 8LB, UK (e-mail: jmw5@st-andrews.ac.uk).

of the drag. Values for the lift and drag of the individual body parts are required for calculations of the power requirements of flapping flight (Wakeling and Ellington, 1997*b*), but it is impossible to resolve them from gliding flight measurements alone.

The forces on dragonfly wings have previously been measured from gliding dragonfly models (Newman *et al.* 1977; Azuma and Watanabe, 1988). Newman *et al.* (1977) made two model gliders with rectangular planform wings but with realistic dragonfly wing cross sections, whereas Azuma and Watanabe (1988) used real dragonfly wings attached to a metal shaft. In both cases, the gliders were trimmed by a movable tail piece and nose weights for stable flights over a range of angles of attack. The glide angles and glide speeds were measured, and the lift and drag thus calculated. This approach is similar to measuring the free gliding flight of dragonflies, except that the drag component of all the non-wing sections can be estimated and subtracted from the total to give the lift and drag of the wings alone. Furthermore, flight parameters such as angle of attack can be controlled by the experimenter. However, the lift and drag forces on a wing are very sensitive to its attitude and camber, and it is unlikely that these model experiments were able accurately to mimic the wing posture adopted by free-flying dragonflies. Okamoto *et al.* (1996) used a variety of techniques, such as force transducer measurements and gliding models with upside-down wings, to create lift-to-drag polars for real dragonfly wings. The present study uses a force transducer to measure the lift and drag on isolated wings and bodies.

Dragonfly and damselfly bodies are long, thin and relatively cylindrical so their aerodynamic performance can be assessed by comparison with the forces acting on cylindrical objects. Ellington (1991) has used a resolved-flow analysis to model the drag on primitive insects by resolving forces into components that are normal and tangential to the body. A similar approach is used here, so that the normal and tangential coefficients of body drag can be compared between the bodies and cylinders. The flow around an object depends on the non-dimensional Reynolds number *Re*:

$$Re = \frac{cV}{\nu}\ , \qquad (1)$$

where c is a characteristic length (body length or mean wing chord), V is the velocity and ν is the kinematic viscosity. This approach has not been verified experimentally for the Reynolds numbers at which insects fly, $Re<5\times10^4$; however, it is well known that the drag on a cylinder normal to flow shows unpredictable 'wobbles' over the range $10^2<Re<10^5$ (Ellington, 1991). The drag coefficients for cylinders of the same length and mean proportions as the dragonfly bodies were also measured for comparative purposes.

Materials and methods

Gliding flight

Sympetrum sanguineum (Müller) and *Calopteryx splendens* (Harris) were collected from Quy Fen and Grantchester Meadows, respectively, between 3 July and 2 August 1994. Following capture, each dragonfly was kept in a plastic box inside a cool dark storage container, and then transferred to a refrigerator at 4 °C once back in Cambridge. All individuals were flown within 24 h of capture.

Gliding flights were filmed in the greenhouse at the Entomology Field Station, University of Cambridge. Down the centre of the building, a pond was dug, measuring 8.9 m by 1.3 m and 0.7 m deep. The design of the pond conformed to guidelines in the publication *Dig a Pond for Dragonflies* by the British Dragonfly Society. The pond was stocked with aquatic plants, both submerged and emergent, taken from local sites, and the borders of the greenhouse were planted with hedgerow plants to provide both perches and shade. Sunlight intensity and thus temperature was reduced by a combination of netting under the apex of the roof and a fine white spray on the glass panels of the greenhouse. During filming, all the doors and vents to the greenhouse were closed to reduce drafts; air currents over the pond measured using a Prosser Science Instruments AVM 502 bead thermistor anemometer were always less than 0.02 m s^{-1}.

Gliding flights were filmed using two Panasonic BL600 video cameras with shutter speed set to 1 ms; 50–70 mm zoom lenses were set to frame the glide area. One camera viewed along the length of the pond, while the other camera viewed perpendicular to this axis. The cameras were positioned 6.9 and 2.5 m, respectively, from the centre of the filming area and were aligned on orthogonal axes. The filming area was 1 m wide and 0.5 m high, and it was marked out by three black rods suspended from the roof by white cotton threads. The rods were 0.8 m apart; two rods were 0.1 m long and the third was 0.3 m long. White sheet screens were placed on the far sides of the pond, so the camera images consisted solely of the black marker rods and the gliding dragonflies. Signals from the two cameras were mixed using a Videomatte VM1 vision mixer so that each frame consisted of views from both cameras, which were thus recorded simultaneously onto Sony KCA-60BRS video tape using a Sony VO-5800PS U-matic video cassette recorder. Images were digitized using a Neotech ImageGrabber24 card in a Macintosh Quadra 650 computer. This card would normally grab from every field on the video cassette, giving a temporal resolution of 20 ms.

The three-dimensional coordinates of the dragonflies were calculated by triangulation (Fig. 1). The 0.8 m separation between the marker rods provided a reference length for each camera, and the angle subtended between the rods was calculated using this separation and the distance of the rods from the camera. Angles to the dragonfly from each camera were calculated from its relative position within the subtended angles. Thus, the camera positions and the angle from each camera to the dragonfly are known, and so the position of the dragonfly within the horizontal plane can be calculated. The side-view camera was positioned so that both it and the bottom of the 0.3 m marker rod were in a horizontal plane, and the

subtended angle to the top of the rod ε was determined. The angle of elevation of the dragonfly above the horizontal, ε′, was calculated from its vertical position relative to the rod. The height of the dragonfly could thus be calculated from its distance to this side camera and its angle of elevation.

At the start of each filming session, the accuracy was tested by rotating a triangular board with sides of 0.3, 0.4 and 0.5 m within the filming area. Calculated positions for the corners showed that a point could be located anywhere within the filming area with a standard error of 0.011 m. This digitising error encompasses both human error and errors introduced by the resolution of the filming system.

Digitized sequences of gliding, where the wings did not flap between frames, were tested to determine the steadiness of each flight. The horizontal positions of the dragonfly along the side-view axis were plotted against the positions along the end-view axis to give the horizontal course for each flight; each point was allotted error bars corresponding to the digitising errors. In all cases, a linear fit could be made within these error bars, and so these flights were assumed to be within a vertical plane. The vertical and horizontal velocities between each digitized field were then plotted against time, with the corresponding velocity error bars. Where there was a linear fit within the error bars for a series of consecutive points (Fig. 2), the gliding flight was assumed to have been at a constant acceleration; the velocity was the mean velocity for those points and the acceleration was the gradient of the least-squares linear fit.

During steady gliding, the kinetic energy of the dragonfly remains constant, and the energy required to overcome the drag of the body and wings comes not from the thrust of beating wings but rather from the loss of height and hence potential energy. When the dragonfly is gliding at an angle θ from the horizontal, the forces can be resolved as shown in Fig. 3A. A lift force L perpendicular to the air velocity V is generated mainly by the wings. The drag force D is parallel to this velocity and is the sum of the parasite drag on the body and the profile and induced drag on the wings. The resultant aerodynamic force must be vertical and of magnitude $m\boldsymbol{g}$, where m is mass and $\boldsymbol{g}$ is the acceleration due to gravity, to balance the weight of the dragonfly.

The lift and drag forces are:

$$L = m\boldsymbol{g}\cos\theta\,, \tag{2}$$

$$D = m\boldsymbol{g}\sin\theta\,, \tag{3}$$

and the glide angle is determined by the ratio of lift and drag:

$$\theta = \arctan(D/L)\,. \tag{4}$$

The glide angle is shallow for good gliders such as dragonflies, allowing some small angle approximations to be made: $\cos\theta \approx 1$ and $\sin\theta \approx \theta$ for θ measured in radians. The equations for lift and drag can thus be reduced to:

$$L \approx m\boldsymbol{g}\,, \tag{5}$$

$$D \approx m\boldsymbol{g}\theta\,, \tag{6}$$

and the glide angle approximates to:

$$\theta \approx (D/L)\,. \tag{7}$$

Given that the weight remains constant, the minimum glide angle θ_{min} is achieved when the total drag is at a minimum, D_{min}. Gliding at θ_{min} maximises the horizontal distance travelled for a given loss of height.

Gliding flight does not, however, have to be steady at a constant velocity. If the resultant aerodynamic force does not balance its weight, then the dragonfly will accelerate in the

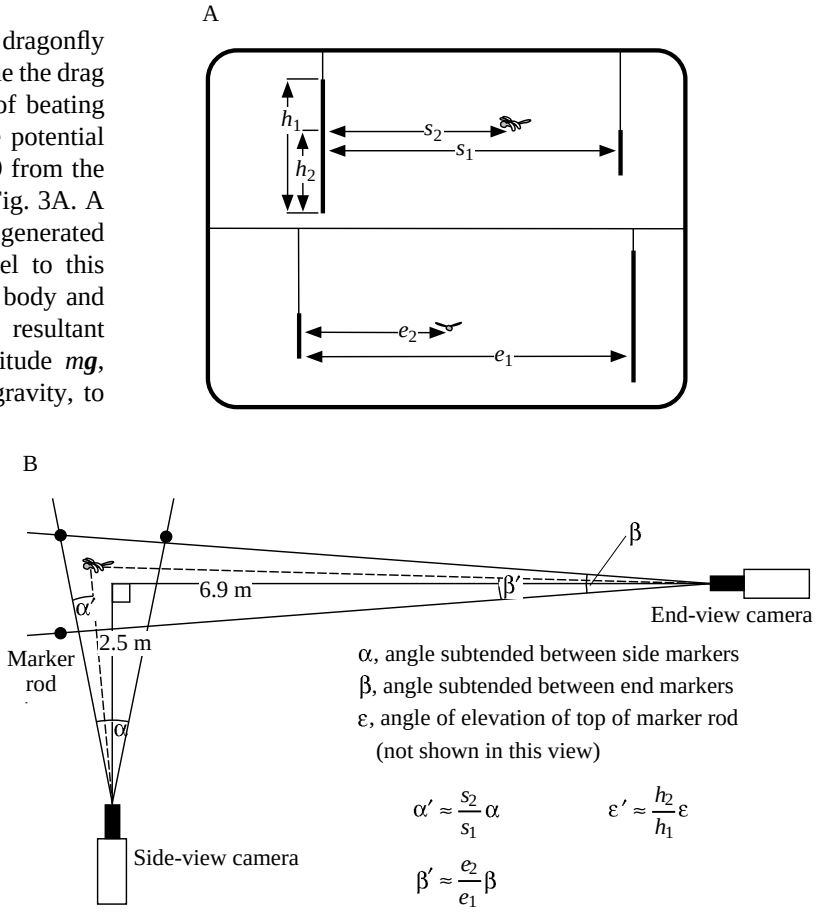

Fig. 1. (A) Diagram of a typical split-screen recorded image of a gliding dragonfly. Signals from two perpendicularly oriented cameras were mixed so that each frame consisted of views from both cameras. The proportional distance of the dragonfly between the three marker rods is taken for each camera view. The height (h), side (s) and end (e) view distances were measured. (B) Top view of the video cameras, with a dragonfly in the filming area. Angles between the cameras and the dragonfly can be calculated, and the position of the dragonfly located by trigonometry.

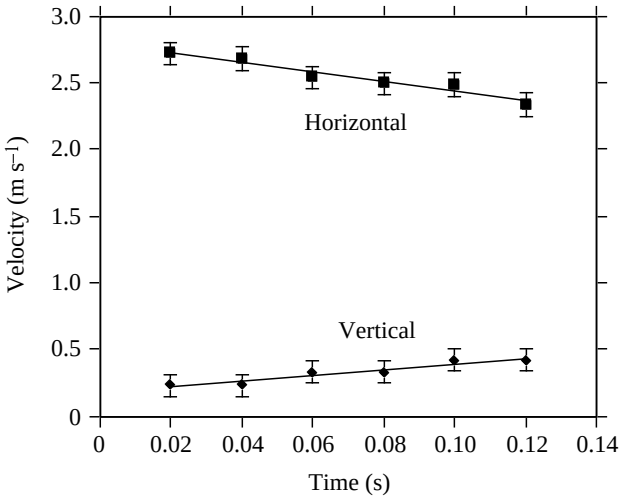

Fig. 2. Least-squares linear regressions and error bars calculated from digitizing errors (see Materials and methods) for vertical and horizontal velocities for glide SSan21.1. Because the linear fit lies between these error bars, accelerations can be assumed to be constant.

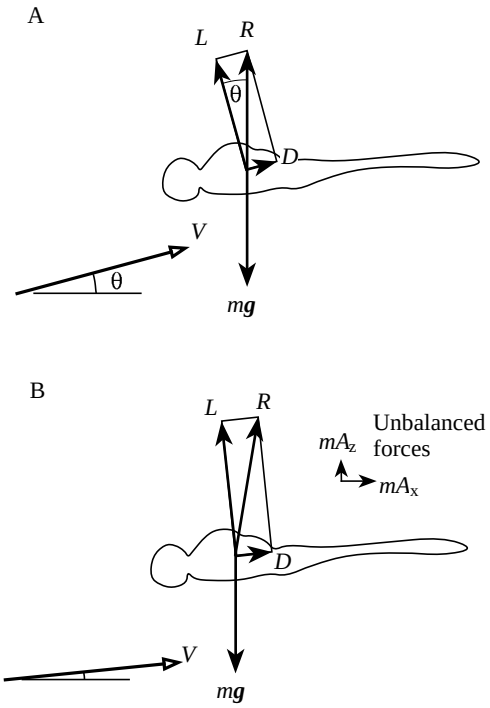

Fig. 3. (A) In steady gliding flight at an angle θ to the horizontal, the lift L and drag D are, respectively, perpendicular and parallel to the air velocity V. The resultant aerodynamic force R balances the weight ($m\boldsymbol{g}$, where m is mass and $\boldsymbol{g}$ is the acceleration due to gravity) of the dragonfly. (B) In accelerated gliding, the forces do not balance the weight, and the dragonfly experiences a backward acceleration A_x and a vertical acceleration A_z.

direction of the unbalanced part of that force (Fig. 3B). For a dragonfly gliding with backward acceleration A_x and upward acceleration A_z, the lift and drag are satisfied by:

$$A_x = \frac{D\cos\theta - L\sin\theta}{m}\ , \tag{8}$$

$$A_z = \frac{L\cos\theta + D\sin\theta}{m} - \boldsymbol{g}\ . \tag{9}$$

These equations can again be reduced for cases where θ is small:

$$A_x \approx \frac{D - L\theta}{m}\ , \tag{10}$$

$$A_z \approx \frac{L + D\theta}{m} - \boldsymbol{g}\ . \tag{11}$$

Horizontal and even upwardly inclined glides ($\theta \leqslant 0$) can occur when the dragonfly decelerates horizontally, using a loss of kinetic energy instead of potential energy to overcome drag. This kinetic energy can even be converted into potential energy, raising the centre of mass in upward gliding flight. The lift and drag forces for $\theta \leqslant 0$ must satisfy the following conditions:

$$L \geqslant m(A_z + \boldsymbol{g})\,, \tag{12}$$

$$D \leqslant mA_x\,. \tag{13}$$

Thus, during accelerated gliding flight there is no longer a limit of the minimum glide angle occurring at D_{min}. Gliding can occur at shallower angles and even be upwardly inclined provided it is accompanied by horizontal decelerations of the dragonfly.

In both steady gliding and accelerated gliding, the lift coefficient C_L is given by:

$$C_L = \frac{2L}{\rho V^2(S_f + S_h)}\ , \tag{14}$$

where ρ is the air density at the temperature relevant to each flight and (S_f+S_h) is the total wing area.

Force measurements

The force transducer and wind-tunnel described by Dudley and Ellington (1990) were used in this study after several modifications had been made to improve the transducer performance. Insect bodies and wings were mounted using insect pins to the bottom of the central shaft, and rotation of the whole transducer about its vertical axis changed the angle of attack. Tunnel velocity was continuously monitored with an Airflow AV-2 rotating vane anemometer. The anemometer and transducer signals were read into a Macintosh Quadra 650 computer *via* a National Instruments NB-MIO-16 12-bit analogue-to-digital converter. The data were processed in a LabView environment in which the mean of 20 consecutive measurements from the analogue-to-digital converter was recorded for each sample.

Dragonfly and damselfly bodies were set in an elongated posture with their legs removed. Nachtigall and Hanauer-

Thieser (1992) measured no difference in parasite drag between honeybees with their legs set in a 'good' flight posture tucked up under the body and honeybees with their legs removed. Flying dragonflies typically tuck their legs under their thorax and, in the present study, the additional drag due to the legs is ignored. The bodies were dried for at least a week, and then mounted onto insect pins passing laterally through the centre of the thorax. The pins were secured in place with a drop of molten beeswax. Fresh bodies were not sufficiently rigid to maintain an elongated posture during measurements. Several fresh bodies were tested with a wire inserted through the length of the abdomen to keep them outstretched; these results did not differ from those for dried bodies.

For both *S. sanguineum* and *C. splendens*, force measurements (N=5) were made for five individuals at body angles α_b of $-20°<\alpha_b<70°$ (where positive body angles indicate a 'nose-up' attitude), and at tunnel velocities of $1<V<5\,m\,s^{-1}$ ($2500<Re<15\,000$). The wide range of body angles was chosen for use in the resolved-flow analysis rather than being representative of body angles during flight. Frontal and planform body areas were measured using a Panasonic BL600 video camera linked to a Macintosh Quadra 650 computer *via* a Neotech ImageGrabber24 board. Cylindrical models of the dragonfly and of the damselfly were also tested; these models were made from wooden dowel and coated with a smooth varnish lacquer. The lengths (and planform areas) of these models were the same as the mean values for *S. sanguineum* and *C. splendens* and were 35.3 mm (88.9 mm^2) and 46.2 mm (88.8 mm^2), respectively. Aerodynamic force was assumed to act along the midline of the bodies.

Wings from freshly killed dragonflies were mounted on a pin using a small drop of beeswax at the ventral surface. Forces were measured with the wings at angles of attack ranging from $-20°<\alpha<70°$ and at tunnel velocities of 2, 3.5 and $5\,m\,s^{-1}$. Wing areas were measured using the same system as for the bodies, and the aerodynamic force was assumed to act through the radius of the first moment of wing area. Wing and morphological parameters for these species and for a further five dragonfly species are published elsewhere (Wakeling, 1997).

The effect on drag of interference between the mounting pin and the dragonfly body was tested in the following way. The drag on four *C. splendens* bodies was measured as described above with the bodies and also with a second pin introduced vertically from below and not quite touching the body. *C. splendens* was chosen because it has a thinner body than *S. sanguineum*, and so any interference from the extra pin may be proportionally greater and thus easier to detect. Each body was tested at body angles of 0° and 90° and at the five velocities used in this study. For each test, measurements (N=20) were made with and without the second pin. Analysis of variance of the drag measurements showed no significant difference (95% confidence level) between the cases for all except one of the tests. The drag measured at Re=3000 and a body angle of 0° was significantly greater with the additional pin than without it; however, the drag increase was small (1.9%) and within the usual level of measurement accuracy. Effects of interference from the mounting pin can thus be ignored.

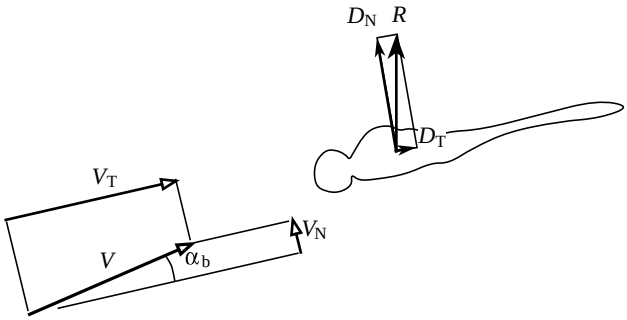

Fig. 4. In the resolved-flow analysis, the air velocity V is resolved into normal V_N and tangential V_T components relative to the longitudinal axis of the body. The angle between this axis and the air velocity is the angle of attack of the body α_b. Normal and tangential drag forces D_N and D_T are calculated from the velocity components, giving the resultant force R.

Resolved-flow analysis

The lift and drag coefficients on a gliding cylindrical body can be modelled using a resolved-flow analysis (Ellington, 1991). The model resolves the velocity V into a component V_N ($=V\sin\alpha_b$) normal to the cylinder and a component V_T ($=V\cos\alpha_b$) tangential to the cylinder, where the cylinder is oriented at an angle α_b to the flow (Fig. 4). The drag forces are estimated for the normal and tangential directions, and then summed into a total force acting on the cylinder. The model assumes that the normal and tangential flow patterns do not interact and can be analysed independently. It also assumes that no circulatory lift is generated, and thus the cylinder does not act as a lifting surface. The unpredictable nature of the wake around cylinders normal to flow precludes detailed analytical approximations of the normal drag coefficient for the range of Re at which dragonflies fly ($10^2<Re<10^5$); however, good agreement between measured forces at laminar Reynolds numbers (Hoerner, 1958) and the resolved-flow analysis have been shown previously (Ellington, 1991). The dragonfly body is particularly suited for this analysis because the body approximates a long thin cylinder which is reasonably circular in cross section throughout its length.

In the analysis, the normal D_N and tangential D_T drag components are expressed as inertial forces:

$$D_N = 0.5\rho A V_N^2 C_N, \quad (15)$$

$$D_T = 0.5\rho A V_T^2 C_T, \quad (16)$$

where C_N and C_T are the respective drag coefficients. The area A is the planform area of the cylinder and is equal to the product of length and mean diameter. Planform area was used in preference to frontal area so that the forces acting on cylinders of different lengths but the same diameter could be

compared. The resultant force R given by D_N and D_T is then resolved into conventional lift and drag forces:

$$L = 0.5\rho AV^2(\sin^2\alpha_b\cos\alpha_b C_N - \cos^2\alpha_b\sin\alpha_b C_T) , \quad (17)$$

$$D = 0.5\rho AV^2(\sin^3\alpha_b C_N + \cos^3\alpha_b C_T) . \quad (18)$$

These lift and drag forces are given in the usual form for inertial forces, and so the lift coefficient C_L and drag coefficient C_D for the gliding body can be expressed by:

$$C_L = \left(\frac{\alpha_b}{|\alpha_b|}\right) \sin^2\alpha_b\cos\alpha_b C_N - \cos^2\alpha_b\sin\alpha_b C_T , \quad (19)$$

$$C_D = |\sin^3\alpha_b| C_N + \cos^3\alpha_b C_T . \quad (20)$$

Using the resolved-flow analysis, the lift and drag forces on a gliding body can thus be modelled knowing only the normal and tangential drag coefficients, which are functions of the Reynolds number based on the diameter and length of the body, respectively. The assumption that the normal and tangential flows are independent requires that these Reynolds numbers are calculated using the corresponding normal and tangential velocities. However, as these assumptions are only approximately true, a further simplification is made: a single value for the Reynolds number is taken using the glide speed and the length of the body.

The inertial form of the resolved-flow equations introduces a small but significant geometrical error for the Reynolds number range appropriate to insect flight. The relationship between drag and velocity is quadratic, in general, giving:

$$D = 0.5\rho A(k_1 V + k_2 V^2) , \quad (21)$$

where k_1 is the coefficient for viscous drag and k_2 is the coefficient for inertial drag. For large Reynolds numbers (Re>10^4), the V^2 term dominates, $C_D \approx k_2$ and the drag is due mainly to inertial forces; drag forces behave as if they vary only with the square of velocity. Most of the data from the aerodynamics literature are in this range, but insects fly at lower Reynolds numbers where the linear term k_1V cannot be ignored. The quadratic relationship at such Re is well known and is conventionally absorbed in the inertial form of the drag equation by a drag coefficient that decreases with increasing Re.

However, consider four new constants a, b, c and d that express the normal and tangential drag forces in the quadratic form:

$$D_N = 0.5\rho A(aV\sin\alpha_b + bV^2\sin^2\alpha_b) , \quad (22)$$

$$D_T = 0.5\rho A(cV\cos\alpha_b + dV^2\cos^2\alpha_b) . \quad (23)$$

The lift and drag coefficients for the gliding body can then be resolved as:

$$C_L = \frac{(a-c)}{V} \sin\alpha_b\cos\alpha_b + \left(\frac{\alpha_b}{|\alpha_b|}\right) b\sin^2\alpha_b\cos\alpha_b - d\cos^2\alpha_b\sin\alpha_b , \quad (24)$$

$$C_D = \frac{a}{V} \sin^2\alpha_b + b|\sin^3\alpha_b| + \frac{c}{V} \cos^2\alpha_b + d\cos^3\alpha_b . \quad (25)$$

Again, it can be seen that coefficients b and d are equivalent to C_N and C_T, respectively, from equations 19 and 20, showing that for high Reynolds numbers these equations provide reliable estimates for the coefficients. The new terms in equations 24 and 25 represent the geometrical influence of the linear terms of the quadratic equations 22 and 23. This influence is significant but is not revealed by the inertial form of the drag equations, which corrects for the changing magnitude of the drag force by a variable C_D. At the speeds at which dragonflies fly and glide, the coefficients a and c become significant in determining the overall lift and drag coefficients. The forces acting on dragonfly bodies may thus be modelled more precisely using these constants a, b, c and d to allow the drag to vary as quadratic functions of velocity and Reynolds number. For comparison with other studies, the normal and tangential coefficients are then expressed as:

$$C_N = \frac{a}{V_N} + b , \quad (26)$$

and

$$C_T = \frac{c}{V_T} + d . \quad (27)$$

Results

Gliding

A typical flight of *S. sanguineum* in the greenhouse consisted of several laps around the pond before it settled on a perch. The perches chosen varied between the emergent vegetation from the pond, the plants around the edge of the greenhouse, and also the green netting along the roof. The latter choice is similar to the behaviour of dragonflies perching in the tree foliage around Quy Fen, from where they were captured. When a dragonfly settled, the perch was agitated to encourage it to fly again. Gliding periods occurred over the surface of the pond, skimming over the vegetation.

The dimensions of the gliding dragonflies are given in Table 1. A more detailed description of wing and body morphologies for this species and a further six Odonatan species has been published elsewhere (Wakeling, 1997).

First observations suggested that periods of gliding lasted

Table 1. *Body dimensions for* Sympetrum sanguineum

Identity	Mass (g)	Wing length (mm)		Wing area (mm^2)	
		Forewing	Hindwing	Forewings	Hindwings
SSan21	137.9	28.0	27.1	358.5	459.0
SSan22	123.8	26.3	25.7	325.2	401.9
SSan24	113.8	27.4	27.1	322.1	415.1
SSan26	115.0	26.7	25.7	302.8	509.9
SSan27	135.2	28.3	27.0	348.6	454.1

Table 2. *Characteristics of glide sequences recorded for* Sympetrum sanguineum

Identity, air temperature (°C)	Glide angle, θ (degrees)	Glide speed, V ($m\,s^{-1}$)	Backwards acceleration, A_x ($m\,s^{-2}$)	Vertical acceleration, A_z ($m\,s^{-2}$)	Lift:drag ratio, L/D	Lift coefficient, C_L
SSan21,	−7.4	2.6	3.5	2.2	6.3	0.56
37.2	6.2	2.1	1.0	−6.7	2.2	0.20
SSan22,	15.4	1.6	4.4	−4.5	0.7	0.50
39.4	26.9	2.0	3.2	2.1	1.1	0.70
SSan24,	34.2	2.0	−1.1	−1.4	2.0	0.53
40.1	36.2	2.2	−1.9	−1.8	2.4	0.43
	33.4	2.1	−1.0	7.8	1.7	0.93
SSan26,	10.6	2.4	3.2	−7.9	0.4	0.06
33.8	3.5	2.1	3.3	−5.8	1.1	0.20
	0.9	1.3	1.5	−8.4	0.9	0.20
	26.4	1.9	1.8	−7.4	0.5	0.09
SSan27,	13.5	0.8	3.6	−7.4	0.4	0.61
32.6	8.4	1.9	3.1	−5.3	1.1	0.33

for up to 0.5 s, covering approximately 1 m; however, analysis of the films showed that the gliding was periodically interrupted by brief wingbeats, with the mean true glide time being 0.13 s and with no period of uninterrupted gliding exceeding 0.20 s. During glide periods, the wings are held in a shallow dihedral; this provides stability against any rolling moments. The dihedral angle was ignored in the gliding analysis, leading to an overestimation of the actual wing area providing weight support and a corresponding underestimation of the lift coefficient, but this bias will introduce an error of less than 5 %.

All the *S. sanguineum* glide sequences occurred within a vertical plane: i.e. there was no instance of turning during gliding flight. The criteria for gliding flight were fulfilled by 13 sequences, and the characteristics of these are summarised in Table 2. The glides performed in this study typically involved a backward and downward accelereration. The gliding flights with an upward acceleration (positive values in Table 2) generally occur when the wings are working at higher lift coefficients. The values for the lift coefficients in Table 2 assume that all the lift is generated by the wings and not the body, and the values represent a mean C_L for both the forewings and the hindwings. These flights do not necessarily include instances of the best L/D ratio or of the maximum lift coefficient $C_{L,max}$.

Wing lift and drag

Lift and drag forces were measured for six fore- and hindwings each from *S. sanguineum* and *C. splendens*. Values for the force coefficients were pooled and means have been plotted as lift-to-drag polars in Figs 5 and 6. Owing to the inevitable variation in setting the wing camber when the wings were mounted, and in assessing the zero angle of attack when attaching them to the transducer, the values for $C_{L,max}$ are likely to be underestimates. At any given angle of attack α, it is unlikely that all six wings are operating at $C_{L,max}$, so the mean value will necessarily be biased low. This problem is not so pronounced for the values of $C_{D,min}$; the polars show that the wings operate near to $C_{D,min}$ for a wide range of angle of attack, and slight deviations in the mounting will have little effect on that mean value.

The polars for *S. sanguineum* at the three different Reynolds numbers are almost identical for both the fore- and hindwings. There seems to be little effect of varying Reynolds number on the lift and drag characteristics of these wings in the range $700<Re<1900$ for the forewings and $900<Re<2400$ for the hindwings; these correspond to the velocity range $2.0\,m\,s^{-1}<V<5.0\,m\,s^{-1}$. There is one slight systematic difference in the polars for different values of *Re*: both the fore- and hindwings show a reduction in C_D ($\alpha=10°$) at the lowest velocity ($V=1\,m\,s^{-1}$) which is not present at the higher velocities and values of *Re*. This drag reduction leads to lift-to-drag ratios that are unusually high for insect wings: $L/D=20.6$ for the forewings and 16.8 for the hindwings. The lift-to-drag ratios remain high for angles of attack of $5°<\alpha<20°$ for both the fore- and hindwings. The polars for *C. splendens* (Fig. 6) were also coincident across this velocity range, which corresponded to $800<Re<2100$. However, unlike *S. sanguineum* wings, there does not appear to be the systematic reduction of C_D at $\alpha=10°$ at the lowest speed. The maximum mean lift-to-drag ratios are $L/D=5.8$ at $\alpha=5°$ for the forewings, and 17.9 at $\alpha=10°$ for the hindwings. High values of L/D persist for $10°<\alpha<20°$ for the forewings and $5°<\alpha<10°$ for the hindwings.

The maximum lift coefficients for *S. sanguineum* were $C_{L,max}=1.05$ for the forewings and $C_{L,max}=1.07$ for the hindwings. The mean values for the range $30°<\alpha<50°$ were $\bar{C}_L=0.99$ for the forewings and $\bar{C}_L=1.02$ for the hindwings. The maximum lift coefficients for *C. splendens* were $C_{L,max}=0.93$ for the forewings and $C_{L,max}=1.15$ for the hindwings. The mean values for the range $30°<\alpha<50°$ were $\bar{C}_L=0.89$ for the forewings and $\bar{C}_L=1.00$ for the hindwings. Values for $C_{L,max}$ are similar for the dragonfly fore- and hindwings, whereas they

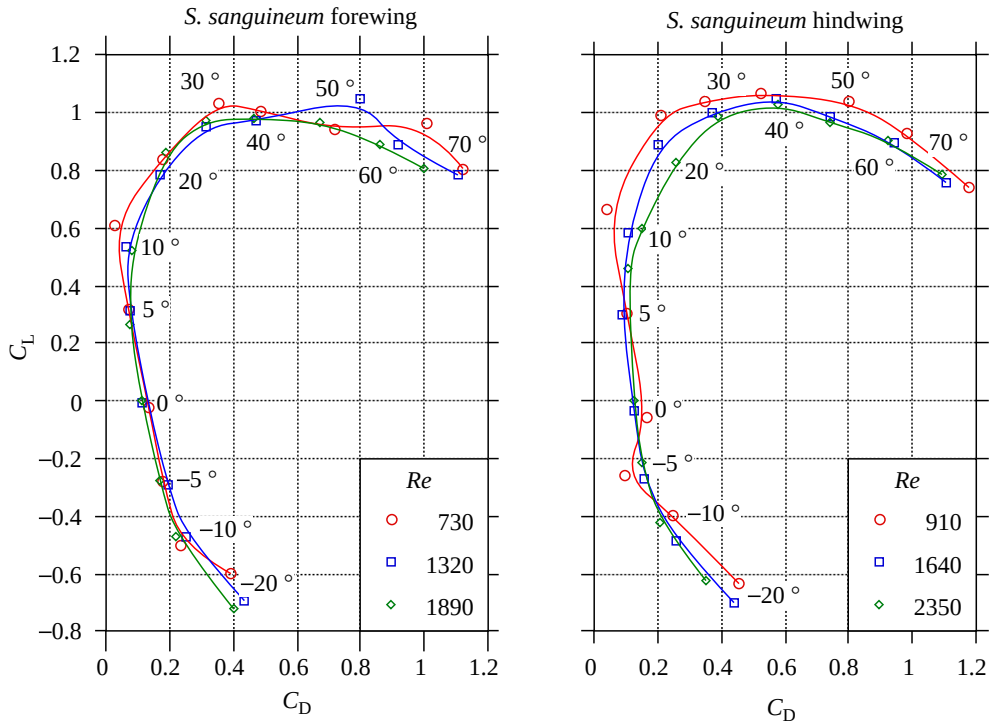

Fig. 5. Polar diagrams for *Sympetrum sanguineum* wings. Each point is the mean from the wings of six individuals. Standard errors were smaller than the symbol size and were as follows: for the forewings $C_{L,error}$<0.012, $C_{D,error}$<0.011; for the hindwings $C_{L,error}$<0.027, $C_{D,error}$<0.018. Lines are Bezier curves adjusted to give a close fit to all the points. *Re*, Reynolds number; C_L, lift coefficient.

differ for the damselfly fore- and hindwings; this is surprising, considering that the shapes of the dragonfly wings are different, whereas in the damselfly they are not.

The total drag on the wings is the sum of the profile drag and the induced drag:

$$D = D_{pro} + D_{ind} . \quad (28)$$

Correspondingly, the drag coefficient at any angle of attack can be taken as the sum of the profile and induced drag coefficients at that angle of attack:

$$C_D(\alpha) = C_{D,pro}(\alpha) + C_{D,ind}(\alpha) . \quad (29)$$

At the zero lift angle, corresponding closely to α=0 ° in this study, the induced drag is also zero, and the drag on the wing consists entirely of the profile drag. These values of the profile drag coefficients are $C_{D,pro}$=0.12 for *S. sanguineum* forewings

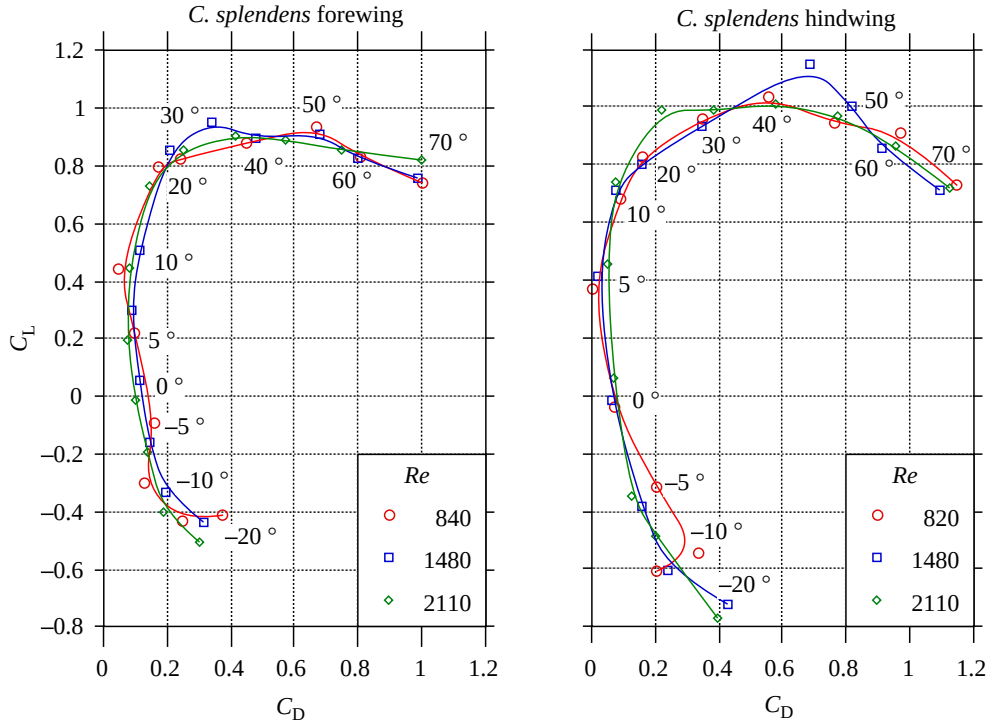

Fig. 6. Polar diagrams for *Calopteryx splendens* wings. Each point is the mean from the wings of six individuals. Standard errors were smaller than the symbol size and were as follows: for the forewings $C_{L,error}$<0.019, $C_{D,error}$<0.018; for the hindwings $C_{L,error}$<0.014, $C_{D,error}$<0.010. Lines are Bezier curves adjusted to give a close fit to all the points.

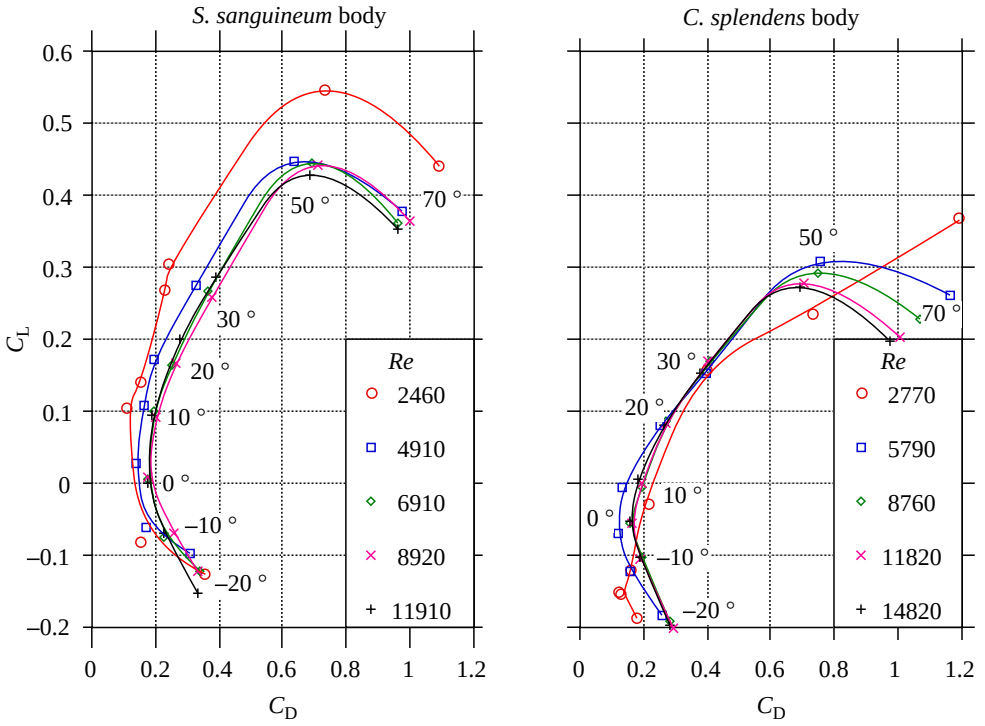

Fig. 7. Polar diagrams for *Sympetrum sanguineum* and *Calopteryx splendens* bodies. Points represent the mean from four bodies for *S. sanguineum* and five bodies for *C. splendens*. Standard errors were smaller than the symbol size and were as follows: for *S. sanguineum* $C_{L,error}$<0.011, $C_{D,error}$<0.011; for *C. splendens* $C_{L,error}$<0.011, $C_{D,error}$<0.027. Lines are Bezier curves adjusted to give a close fit to all the points.

and $C_{D,pro}$=0.14 for the hindwings, and for *C. splendens* $C_{D,pro}$=0.12 for the forewings and $C_{D,pro}$=0.07 for the hindwings.

Body drag

The lift and drag forces were measured for four *S. sanguineum* and five *C. splendens* bodies. The velocity range was 1 m s^{-1}<*V*<5 m s^{-1}, corresponding to 2400<*Re*<11 900 for the dragonfly and 2800<*Re*<14 800 for the damselfly. For each angle of attack, the mean C_L and C_D values (based on planform area) for each species were calculated, and these have been plotted as polars in Fig. 7. To convert these drag coefficients to C_D based on frontal areas they should be multiplied by 3.07 for *S. sanguineum* and 4.16 for *C. splendens*. For each species, the measured force coefficients are similar for velocities greater than 2 m s^{-1}. At the lower velocities, however, systematic deviations do occur. Both *S. sanguineum* and *C. splendens* show higher values for C_L and C_D at the lowest velocity and the largest angles of attack.

Resolved-flow analysis – drag prediction

Graphs of drag coefficient against angle of attack were plotted for each individual dragonfly and damselfly body at each speed tested, and also for the rod model of the dragonfly bodies. The data were fitted, using a non-linear least-squares method, to two equations:

$$C_D = C_N|\sin^3(\alpha_b - \omega)| + C_T\cos^3(\alpha_b - \omega)\,, \qquad (30)$$

and

$$C_D = \frac{a}{V}\sin^2(\alpha_b - \omega) + b|\sin^3(\alpha_b - \omega)| + \frac{c}{V}\cos^2(\alpha_b - \omega) + d\cos^3(\alpha_b - \omega)\,. \qquad (31)$$

Equation 30 corresponds to the resolved-flow analysis by Ellington (1991), and equation 31 is the new model to be tested here. These equations differ from equations 20 and 25 only by an offset angle ω for the body, which accounts for slight variations when aligning the bodies on the force transducer.

The fitted lines from equation 30 systematically overestimated C_D for body angles in the region −10 °<α_b<10 °, as illustrated in Fig. 8A. At these small body angles, the normal component of the velocity is small, and the linear term in the quadratic drag relationship is not negligible compared with the squared term. The additional coefficients *a* and *c* in equation 31 cater for the geometric effect of linear terms, which is particularly important for the normal drag; equation 31 provided a much tighter fit for all the graphs (e.g. Fig. 8A), and there was no systematic deviation of the fit within the range of body angles tested, −20 °<α_b<70 °.

Once initial tests had shown that the drag coefficients from individual bodies could be modelled using the resolved-flow analysis, data were pooled so that each new set contained the data for five individuals over the range of body angles but at one velocity. Again, equation 31 gave a much closer fit than equation 30. Values for C_N and C_T as calculated from equations 31, 26 and 27 are given in Table 3, along with the standard errors of the data points from the fitted lines. The values for C_N and C_T are calculated for normal (α_b=90 °) and tangential (α_b=0 °) flows, respectively.

The resolved coefficients C_N and C_T both vary with Reynolds number. Ellington (1991) gives general ‘global’ relationships which approximate these

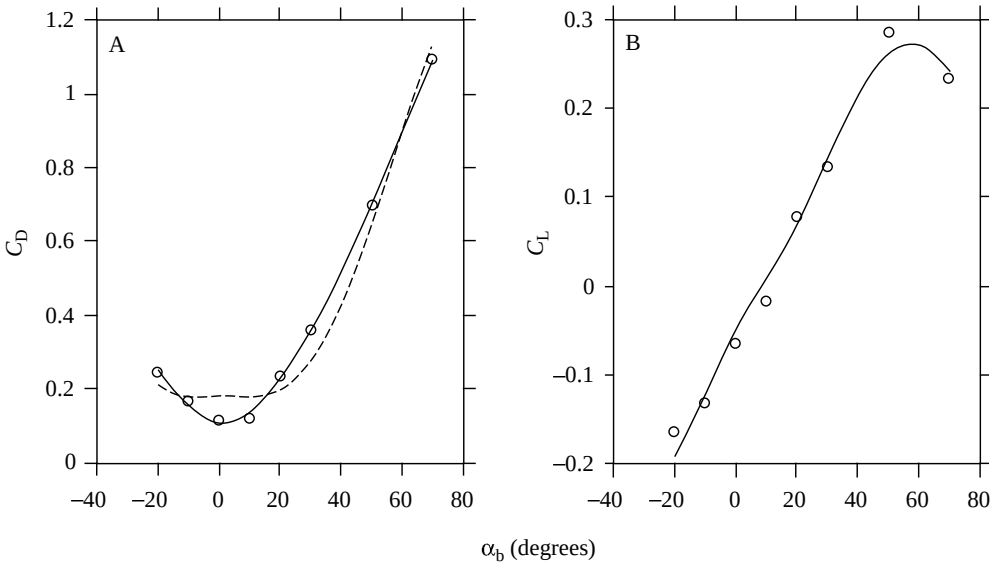

Fig. 8. Pooled values for the drag coefficient C_D and the lift coefficient C_L plotted against body angle α_b for *Calopteryx splendens* at *Re*=5790. Points represent the mean from five bodies. Standard errors were smaller that the symbol size and were as follows: $C_{D,error}$=0.013; $C_{L,error}$=0.010. (A) The fits to C_D are calculated from equation 30 (dashed line) and equation 31 (solid line). (B) The fit to C_L is calculated from equation 36.

coefficients for cylinders over a wide range of *Re*, and these are:

$$C_{N(l/d=\infty)} = 1.1 + \frac{22}{Re} , \quad (32)$$

and

$$C_T = \frac{1.33\pi}{\sqrt{Re}} + \frac{2\pi(l/d)}{Re} , \quad (33)$$

where (l/d) is the length-to-diameter ratio of the cylinder. The coefficients vary with the length-to-diameter ratio and, for comparative purposes, all coefficients have been adjusted to l/d=20 using corrections according to Ellington (1991):

$$\frac{C_N}{C_{N(l/d=20)}} = \frac{0.57 + 0.34e^{(-7.6d/l)}}{0.8025} , \quad (34)$$

Table 3. *Best-fit coefficients for describing drag on dragonfly bodies*

	Re	C_N	C_T	S.E.M.
Sympetrum sanguineum	2460	1.371	0.339	0.075
	4910	1.125	0.132	0.078
	6910	1.106	0.173	0.075
	8920	1.135	0.181	0.075
	11910	1.084	0.179	0.073
Calopteryx splendens	2270	1.701	0.354	0.098
	5790	1.228	0.104	0.063
	8760	1.117	0.148	0.062
	11820	1.135	0.161	0.060
	14820	1.028	0.146	0.059

Re, Reynolds number; C_N, normal drag coefficient; C_T, tangential drag coefficient.

and

$$\frac{C_T}{C_{T(l/d=20)}} = \frac{4.18\sqrt{Re} + 6.28(l/d)}{4.18\sqrt{Re} + 125.66} . \quad (35)$$

The final adjusted results are shown in Fig. 9.

The rod models and the dragonfly bodies show a variation of C_N and C_T with *Re* which is broadly similar to the global trends from a much wider range of *Re*, but there are significant quantitative and qualitative differences. Until there is a better understanding of the flows around such shapes at intermediate *Re*, a suitable analytical expression cannot be fitted to the results. They are thus left here as simple values relevant to each velocity tested. The overall drag coefficient is modelled instead by using the coefficients from Table 3 and equation 25; such predictions fit the dragonfly body data with a standard error of 0.6 % of $C_{D,max}$. For intermediate *Re*, the coefficients must be interpolated from Table 3.

Resolved-flow analysis – lift prediction

The equivalent form of equation 31 to find the best non-linear least-squares fit to the lift coefficient data is:

$$C_L = \frac{a-c}{V}\sin(\alpha_b-\omega)\cos(\alpha_b-\omega) + \left(\frac{\alpha_b-\omega}{|\alpha_b-\omega|}\right) b\sin^2(\alpha_b-\omega)\cos(\alpha_b-\omega) - d\cos^2(\alpha_b-\omega)\sin(\alpha_b-\omega) , \quad (36)$$

and is shown in Fig. 8B. It should be noted that the least-squares fit calculates the best value for (a–c), but will not resolve this quantity further into its component parts.

The best-fit coefficients differed from those generated by equation 31 and the C_D data. Values for (a–c) and for d from the C_L fit were greater than their C_D counterparts. More

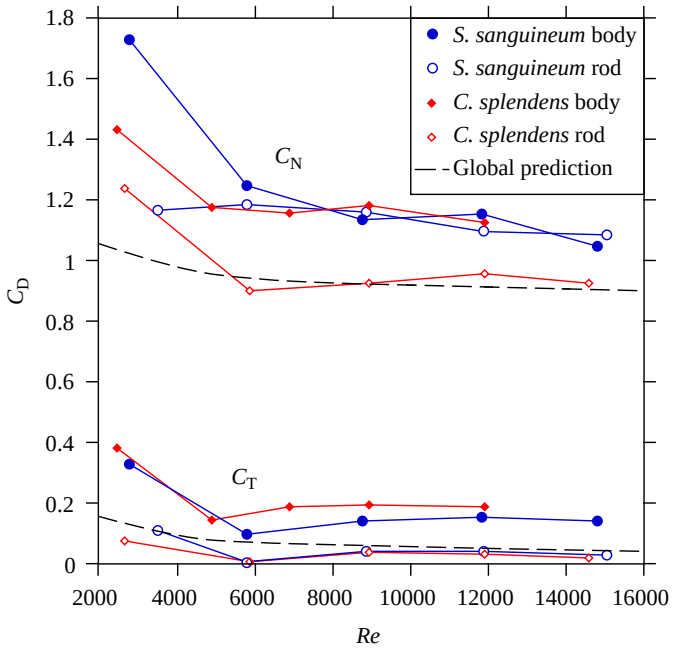

Fig. 9. Normal C_N and tangential C_T drag coefficients C_D plotted against Reynolds number *Re* for the dragonfly bodies, for the dragonfly body models and for the global predictions (Ellington, 1991). Drag coefficients are adjusted to a length-to-diameter ratio of 20 according to equations 34 and 35. Standard errors are smaller than the symbol size.

critically, the values for *b* were sometimes negative; this is mathematically correct but is in reality impossible.

The values for *a*, *b*, *c* and *d* calculated from the drag coefficients and equation 31 were then used in equation 36 to examine how well they fitted the measured lift coefficients. For the dragonfly, the damselfly and the rods, at all velocities tested, the predicted C_L/α_b slope was steeper than the data at small body angles ($-20° < \alpha_b < 20°$). The model also underestimated $C_{L,max}$ for *S. sanguineum* at *Re*>6000, and overestimated $C_{L,max}$ for *S. sanguineum* at *Re*<6000 and for *C. splendens* at all Reynolds numbers (results not shown).

The resolved-flow analysis provides a reliable prediction for the drag coefficient for the dragonfly and damselfly bodies. It does not, however, provide a good model for the lift coefficient. One or more of its assumptions must be sufficiently incorrect to cause such significant errors.

Discussion

Consider a typical *S. sanguineum* gliding at 2 m s^{-1}. It is of average build, with body parameters being the mean of those for this species. Its lift and drag coefficients are taken from the polars in Figs 5 and 7 for wing and body angles at an arbitrary 10°. The lift and drag forces generated by its wings and body are expressed as a fraction of its body weight in Table 4. The lift generated by the body whilst gliding is insignificant compared with the lift generated by the wings. It is thus a reasonable approximation during the gliding flight calculations

Table 4. *Lift and drag forces acting on* Sympetrum sanguineum *whilst gliding at 2 m s^{-1}, expressed as fractions of body weight*

	L/m***g***	*D*/m***g***
Forewings	0.38	0.07
Hindwings	0.49	0.08
Body	0.02	0.03

to attribute the entire lift produced by the dragonfly to its wings and to calculate the lift coefficient purely from the wing area. Body drag, however, makes a significant contribution to the total drag on the dragonfly. These drag components cannot be resolved from the gliding flights alone, and so drag coefficients were not calculated for the gliding sequences.

During gliding, as in all flight, there are two velocities at which the power requirements for that flight are minimised. These velocities minimise the power consumed per unit time, or the power consumed per unit distance, and can be calculated using equations from Ennos (1989). The energy expenditures during prolonged steady gliding in *S. sanguineum* are thus minimised over the range 0.6 m s^{-1}<*V*<0.9 m s^{-1}. These 'optimum' speeds, however, are considerably slower than the glide speeds measured in the present study. These glides involved accelerations and were only for brief periods, so may not be comparable with predictions of optimal speeds for sustained gliding. Glide speeds may alternatively be chosen for optimising the encounter rate with prey or conspecifics. Gliding for any duration will allow convective cooling from the thorax (Church, 1960; Casey, 1976; May, 1976) without excessive heat production from the flight muscles and so may be advantageous for thermoregulation. The bursts of flapping during gliding may serve to maintain a high flight velocity which the dragonfly may resume at the end of its glide.

The high lift coefficient C_L=0.93 that was calculated from the gliding flights (Table 2) and the values for C_{Lmax} obtained from the isolated wings (1.05 and 1.07 for *S. sanguineum*, and 0.93 and 1.15 for *C. splendens*; Figs 5, 6) are similar to those measured for other dragonflies. Lift and drag measurements on model aeshnid dragonfly wings (Newman *et al.* 1977) over the range 12 000<*Re*<60 000 gave $C_{L,max}$=0.96. Measurements have also been made on real *Anax parthenope* wings with $C_{L,max}$=1.05 (Okamoto *et al.* 1996), yielding a polar diagram very similar to the ones presented here for *S. sanguineum*. Rudolph (1976) has measured $C_{L,max}$ as 0.85 for *C. splendens* forewings; this value is lower than that recorded here.

Apart from the high lift coefficient measured for the locust *Schistocerca gregaria* forewing, $C_{L,max}$=1.3 (Jensen, 1956), all other values of $C_{L,max}$ for insects are substantially lower than those for dragonflies: i.e. the cranefly *Tipula oleracea* ($C_{L,max}$=0.86), the fruitfly *Drosophila virilis* ($C_{L,max}$=0.87), the bumblebee *Bombus terrestris* ($C_{L,max}$=0.69) and the hawkmoth *Manduca sexta* ($C_{L,max}$=0.71) (Nachtigall, 1977; Vogel, 1967; Dudley and Ellington, 1990; Willmott, 1995, respectively).

The reason for these other insect wings generating less lift is neither an aspect ratio AR nor a Reynolds number phenomenon, as shown by the large range used for both these values: *Tipula oleracea* (AR=11, Re=1500), *Drosophila virilis* (AR=2, Re=200), *Bombus terrestris* (AR=7, Re=500–1200), *Manduca sexta* (AR=5, Re=1000–5500). Nor is poor wing performance purely related to small size, as the hawkmoth with the worst-performing wings is by far the largest of the above insects. Dragonfly wings appear to have an exceptional ability to produce lift under steady conditions compared with those from most other insects.

The measured values for profile drag, $C_{D,pro}$, are 0.12 and 0.14 for *S. sanguineum* and 0.12 and 0.07 for *C. splendens* fore- and hindwings, respectively. These compare well with values for other large insects: $C_{D,pro}$ was 0.11 for *C. splendens* forewings (Rudolph, 1976), 0.09 for *Anax parthenope* fore- and hindwings (Okamoto *et al.* 1996) and 0.05 and 0.07 for flat and cambered locust forewings (Jensen, 1956). The Blasius equation describes the skin friction over a flat plate in perfect laminar flow; this is the absolute minimum value for the profile drag and takes the form:

$$C_D = \frac{2.66}{\sqrt{Re}} . \quad (37)$$

In the Reynolds number range of the wings tested here, this minimum C_D is between 0.05 and 0.09, and so the measured $C_{D,pro}$ values are close to those predicted for the skin friction on flat plates. Ellington (1984*a*), using Vogel's (1967) data for *Drosophila virilis* at $60<Re<200$, suggests that the relationship:

$$C_{D,pro} = \frac{4.8}{\sqrt{Re}} \quad (38)$$

may be more appropriate to model $C_{D,pro}$ for insect wings. This equation predicts $0.10<C_{D,pro}<0.17$ over the range of Reynolds numbers tested, and so gives a reasonable extrapolation to the profile drag at Re values more appropriate to dragonfly flight, although slightly high.

The L/D ratios are high for both the dragonfly and the damselfly wings, because of high values of C_L and low values of C_D, with a noteworthy apparent drag reduction for the dragonfly wings at small positive angles of attack. Polars for model dragonfly wings (Newman *et al.* 1977) show similar features, with an L/D of 11.5; Newman *et al.* (1977) state that the lift curve slope ($dC_L/d\alpha$) is larger than the theoretical value and can be attributed to separation bubbles changing the effective wing profile as the angle of attack increases. Dragonfly polars measured by Okamoto *et al.* (1996) do not show a drag reduction at small angles of attack, and their L/D ratios are 6 and 6.5 for the fore- and hindwings, respectively. Lift-to-drag ratios may not be a very reliable performance indicator of dragonfly wings because measurement errors in the the low drag values at small α will be magnified in the L/D ratio.

The glide performance of the dragonfly can be predicted by calculating the total lift and drag forces on all four wings and the body. For example, with values of C_L=0.8 and C_D=0.15 for both the fore- and hindwings ($\alpha\approx20°$), C_D=0.2 for the body ($\alpha_b\approx20°$), and a glide speed of $2\,m\,s^{-1}$, the L/D ratio for such a glide is 4.6 and it would support a 143 mg dragonfly. These values closely match the actual glide performance of *S. sanguineum* in the greenhouse, and so the lift-to-drag polars presented in the present paper are realistic descriptions of the steady-state aerodynamic performance of the wings and body. It should be noted that this predicted lift-to-drag ratio is for the whole animal, calculated from the lift on the wings and the drag on both the wings and the body; it will thus be lower than L/D for isolated wings.

The polars for the fore- and hindwings of *S. sanguineum* at different Reynolds numbers are more similar than those of *C. splendens*. This is despite the fact that the zygopterous *C. splendens* has fore- and hindwings of the same shape, whereas those of the anisopterous *S. sanguineum* are different. Therefore, the wing shape is unlikely to be a major factor influencing the aerodynamic performance of the wings. Jensen (1956) suggested that structures within the boundary layer should have little influence on the flow characteristics across the wing; however, there is a growing body of evidence to suggest that fine structures on a wing surface can affect its aerodynamic performance. Backflow within a boundary layer can lead to vortices and a change in the general pattern of flow (Prandtl and Tietjens, 1957). Vogel (1967) suggests that microtrichia on the wing surface of *Drosophila virilis* may help to channel the flow and prevent stalling, although Dickinson and Götz (1993) could not repeat these results. Corrugations on the dragonfly wing may trap vortices that alter the effective profile of the wing (Newman *et al.* 1977), and the leading-edge costa may also improve wing performance (Hertel, 1966; Newman *et al.* 1977). Spines occur on the wing veins of all dragonflies (Hertel, 1966; d'Andrea and Carfi, 1988, 1989), but these are shorter than the critical length at which surface roughness affects flow (Schlichtling, 1968). Recent tests on model dragonfly wings have shown that $C_{L,max}$ can be increased by introducing surface corrugation, a thinner leading edge and camber to the wing (Okamoto *et al.* 1996). The wing performance may therefore be finely tuned by the surface structure and may not reflect the overall wing shape *per se*. This study has not attempted to characterise the structure for the four types of dragonfly wing, but such information is needed before further conclusions can be drawn.

The resolved drag coefficients from the rod model bodies were similar to values predicted from empirical relationships derived for cylinders over a much larger range of Reynolds number. However, there were systematic differences, presumably due to peculiarities in the wake flows around cylinders that are not catered for by the global relationship. The drag coefficients from the dragonfly bodies were, in general, higher than those for the rods (see Fig. 9). The rods were of

uniform diameter throughout their length, whereas dragonfly bodies have an enlarged thorax which increases both the normal and tangential drag components. Additionally, the thoraces of both *S. sanguineum* and *C. splendens* are covered with 0.5–0.7 mm hairs; these hairs are long enough to penetrate the boundary layer and so to affect the flows around the body significantly (Schlichtling, 1968). The mean length-to-diameter ratio and planform areas of the bodies were based on measurements that excluded the effective area of these hairs, and so the actual drag is likely to be greater than that predicted from the measured shape alone.

At high *Re*, C_N is dominated by inertial pressure drag. However, at $Re<1000$, viscous drag becomes important and C_N increases. The increase in C_N for dragonfly bodies at $Re<6000$ is probably not due to viscous drag but rather to the nature of vortex shedding into a Karman wake which produces 'wobbles' from the global trend, as illustrated by Ellington (1991). Tangential drag on a cylinder is mainly caused by viscous drag. A notable feature for both the bodies and the rods in this study is that they show a systematic lowering of C_T at $Re\approx6000$. This corresponds to velocities of approximately $2\,m\,s^{-1}$, typical of the flight velocities for these dragonflies (Wakeling and Ellington, 1997*a*). During forward flight, dragonflies typically align their bodies to face the direction of travel, and thus the body drag is mainly due to tangential forces. These two species match their forward flight speeds to a velocity at which C_T is minimal, hence reducing body drag. However, the power cost required to overcome body drag is only a very small fraction of the total power expenditure during flight (Wakeling and Ellington, 1997*b*) and so this saving may be negligible.

The resolved-flow analysis clearly illustrates how the body drag coefficients vary as a function of both body angle and Reynolds number. At higher Reynolds numbers ($Re>6000$), the drag coefficients are reasonably independent of *Re* and the approximation that they vary only as a function of body angle is sufficient. *S. sanguineum* and *C. splendens* typically fly with their bodies in a lower Reynolds number regime, however, and in such cases the dependence of drag coefficients on *Re* is important.

The resolved-flow analysis provides an exceptional fit to the drag data at each velocity, suggesting that the drag model is very reliable. The lift and drag forces were measured simultaneously on shared orthogonal axes, and it can be presumed that the lift and drag data are of similar quality. Therefore, the failure of the resolved-flow analysis to describe the lift coefficients adequately is likely to be due to the analysis rather than the data. Fortunately, it is much more important to model the drag coefficients of the body than the lift coefficients. Table 4 shows that the lift produced by the body of a gliding dragonfly is an insignificant proportion of the overall lift, whereas the drag is a significant component of the total drag. It is only necessary to predict the body C_D for the aerodynamic power calculations (Wakeling and Ellington, 1997*b*), and thus the model does provide a useful tool for describing dragonfly flight.

References

AZUMA, A. AND WATANABE, T. (1988). Flight performance of a dragonfly. *J. exp. Biol.* **137**, 221–252.

CASEY, T. M. (1976). Flight energetics in sphinx moths: heat production and heat loss in *Hyles lineata* during free flight. *J. exp. Biol.* **64**, 545–560.

CHURCH, N. S. (1960). Heat loss and the body temperature of flying insects. II. Heat conduction within the body and its loss by radiation and convection. *J. exp. Biol.* **37**, 186–212.

CORBET, P. S. (1983). *A Biology of Dragonflies*. Farrington, Oxon: E. W. Classey.

D'ANDREA, M. AND CARFI, S. (1988). Spines on the wing veins in Odonata. 1. Zygoptera. *Odonatologica* **17**, 313–335.

D'ANDREA, M. AND CARFI, S. (1989). Spines on the wing veins in Odonata. 2. Anisozygoptera and anisoptera. *Odonatologica* **18**, 147–178.

DICKINSON, M. H. AND GÖTZ, K. G. (1993). Unsteady aerodynamic performance of model wings at low Reynolds numbers. *J. exp. Biol.* **174**, 45–64.

DUDLEY, R. AND ELLINGTON, C. P. (1990). Mechanics of forward flight in bumblebees. II. Quasi-steady lift and power requirements. *J. exp. Biol.* **148**, 53–88.

ELLINGTON, C. P. (1984*a*). The aerodynamics of hovering insect flight. IV. Aerodynamic mechanisms. *Phil. Trans. R. Soc. Lond. B* **305**, 79–113.

ELLINGTON, C. P. (1984*b*). The aerodynamics of hovering insect flight. VI. Lift and power requirements. *Phil. Trans. R. Soc. Lond. B* **305**, 145–181.

ELLINGTON, C. P. (1991). Aerodynamics and the origin of insect flight. *Adv. Insect Physiol.* **23**, 171–210.

ENNOS, A. R. (1989). The effect of size on the optimal shapes of gliding insects and seeds. *J. Zool., Lond.* **219**, 61–69.

HANKIN, E. H. (1921). The soaring flight of dragonflies. *Proc. Camb. phil. Soc.* **20**, 460–465.

HEINRICH, B. (1993). *The Hot-Blooded Insects: Strategies and Mechanisms of Thermoregulation*. Cambridge, MA: Harvard University Press.

HERTEL, H. (1966). Membranous wing of insects. In *Structure – Form – Movement* New York: Reinhold. pp. 78–87.

HOERNER, S. F. (1958). *Fluid-dynamic Drag*. Bricktown, NJ: S. F. Hoerner.

JENSEN, M. (1956). Biology and physics of locust flight. III. The aerodynamics of locust flight. *Phil. Trans. R. Soc. Lond. B* **239**, 511–552.

MAY, M. L. (1976). Thermoregulation and adaptation to temperature in dragonflies (Odonata: Anisoptera). *Ecol. Monogr.* **46**, 1–32.

MAY, M. L. (1978). Thermal adaptations of dragonflies. *Odonatologica* **7**, 27–47.

MAY, M. L. (1995). Dependence of flight behaviour and heat production on air temperature in the green darner dragonfly, *Anax junius* (Odonata: Aeshnidae). *J. exp. Biol.* **198**, 2385–2392.

NACHTIGALL, W. (1977). Die aerodynamische Polare des Tipula-Flugels und eine Einrichtung zur halbautomatischen Polarenaufnahme. In *The Physiology of Movement; Biomechanics* (ed W. Nachtigall), pp. 347–352. Stuttgart: Fisher.

NACHTIGALL, W. AND HANAUER-THIESER, U. (1992). Flight of the honeybee. V. Drag and lift coefficients of the bee's body; implications for flight dynamics. *J. comp. Physiol.* B **162**, 267–277.

NEWMAN, B. G., SAVAGE, S. B. AND SCHOUELLA, D. (1977). Model tests on a wing section of an *Aeschna* dragonfly. In *Scale Effects*

in Animal Locomotion (ed. T. J. Pedley), pp. 445–477. London: Academic Press.

OKAMOTO, M., YASUDA, K. AND AZUMA, A. (1996). Aerodynamic characteristics of dragonfly wings and body. *J. exp. Biol.* **199**, 281–294.

OSBORNE, M. F. M. (1951). Aerodynamics of flapping flight with application to insects. *J. exp. Biol.* **28**, 221–245.

POLCYN, D. M. (1988). The thermal biology of desert dragonflies. PhD thesis, University of California, Riverside.

PRANDTL, L. AND TIETJENS, O. G. (1957). *Applied Hydro- and Aeromechanics*. New York: Dover.

RUDOLPH, R. (1976). Die Aerodynamischen Eigenschaften von *Calopteryx splendens* (Harris) (Zygoptera: Calopterygidae). *Odonatologica* **5**, 383–386.

SCHLICHTLING, H. (1968). *Boundary-Layer Theory*, 6th edn. New York: McGraw-Hill.

SPEDDING, G. R. (1992). The aerodynamics of flight. In *Mechanics of Animal Locomotion* (ed. R. McN. Alexander), pp. 51–111. New York: Springer-Verlag.

VOGEL, S. (1967). Flight in *Drosophila*. III. Aerodynamic characteristics of fly wings and wing models. *J. exp. Biol.* **46**, 431–443.

WAKELING, J. M. (1997). Odonatan wing and body morphologies. *Odonatologica* **26**, 35–52.

WAKELING, J. M. AND ELLINGTON, C. P. (1997*a*). Dragonfly flight. II. Velocities, accelerations and kinematics of flapping flight. *J. exp. Biol.* **200**, 557–582.

WAKELING, J. M. AND ELLINGTON, C. P. (1997*b*). Dragonfly flight. III. Quasi-steady lift and power requirements. *J. exp. Biol.* **200**, 583–600.

WEIS-FOGH, T. (1973). Quick estimates of flight fitness in hovering animals, including novel mechanisms for lift production. *J. exp. Biol.* **59**, 169–230.

WILLMOTT, A. P. (1995). The mechanics of hawkmoth flight. PhD thesis, Cambridge University.